Author(s): Boriouchkine, Alexandre & Sharifi, Vida & Swithenbank, Jim & Jämsä-Jounela, Sirkka-Liisa

Title: Experiments and modeling of fixed-bed debarking residue pyrolysis: The effect of fuel bed properties on product yields

Year: 2015

Version: Post print

Please cite the original version:

Boriouchkine, Alexandre & Sharifi, Vida & Swithenbank, Jim & Jämsä-Jounela, Sirkka-Liisa. 2015. Experiments and modeling of fixed-bed debarking residue pyrolysis: The effect of fuel bed properties on product yields. Chemical Engineering Science. Volume 138. 581-591. ISSN 0009-2509 (printed). DOI: 10.1016/j.ces.2015.07.055.

Experiments and modeling of fixed-bed debarking residue pyrolysis: the effect of fuel bed properties on product yields

Alexandre Boriouchkine*[a], Vida Sharifi[b], Jim Swithenbank[b], Sirkka-Liisa Jämsä-Jounela[a],

a School of Chemical Technology, Aalto University, P.O. Box 16100, 00076 Aalto, Finland (*corresponding author; e-mail: alexandre.boriouchkine@aalto.fi)

b Department of Chemical and Biological Engineering, The University of Sheffield, Mappin Street, Sheffield, S1 3JD

Abstract

This paper presents a study on the fixed-bed pyrolysis of debarking residue obtained from Norway spruce. Analysis is based on the dynamic model of packed bed pyrolysis which was calibrated by determining appropriate reaction rates and enthalpies to match the model predictions with the experimental data. The model comprises mass, energy and momentum equations coupled with a rate equation that describes both the primary and secondary pyrolysis reactions. The experiments used for the model calibration determined the yields of solid, liquid and gaseous pyrolysis products as well as their compositions at three distinct holding temperatures. Subsequently, the dynamic model was used to predict the product yields and to analyze the underlying phenomena controlling the overall pyrolysis reaction in a fixed-bed reactor.

Keywords: woody biomass, pyrolysis modeling, pyrolysis experiments, Norway spruce debarking residue, fixed-bed pyrolysis, pyrolysis product yields

NOMENCLATURE

A_m	pre-exponential factor for component m (1/s)
C_p	heat capacity of the bed (J/(kg·K))
$C_{p,c}$	heat capacity of char (J/(kg·K))

23	$C_{p,w}$	heat capacity of wood (J/(kg·K))
24	d_{cavity}	average pore diameter in the wood particle (m)
25	D_p	particle diameter (m)
26	ε	emissivity coefficient
27	E_m	activation energy for component m (kJ/mol)
28	i	chemical specie
29	k	iteration number
30	n	total number of the measurements
31	k_{bed}	effective heat conduction coefficient of the packed bed (W/(m·K))
32	k_{fiber}	heat conductivity of wood fiber (W/(m·K))
33	k_g	heat conductivity of the gas (W/(m·K))
34	k_m	reaction rate coefficient for component m (1/s)
35	k_{max}	maximum heat transfer coefficient (W/(m·K))
36	k_{min}	minimal heat conduction coefficient (W/(m·K))
37	k_{rs}	void-to-void heat conduction coefficient (W/(m·K))
38	k_{rv}	solid surface-to-solid surface heat conduction coefficient (W/(m·K))
39	$k_{s,eff}$	heat conduction coefficient of the solid matter (W/(m·K))
40	$k_{s,rad}$	heat radiation coefficient of the solid matter (W/(m·K))
41	m_m	predicted weight of component *m* (kg)
42	m_{meas}	measured sample weight (kg)

43	r	cylindrical coordinate (m)
44	T	temperature of the solid (K)
45	t	time variable (s)
46	α_m	initial mass fraction of the component in a wood sample
47	ρ	total mass concentration of the fuel bed (kg/m^3)
48	ρ_c	mass concentration of char (kg/m^3)
49	ρ_w	mass concentration of volatiles (kg/m^3)
50	τ	tortuosity
51	σ_c	pore constriction factor
52	σ	Stefan-Boltzman constant (W/(m^2·K^4))
53	u	velocity vector
54	μ	fluid viscosity
55	I	identity matrix
56	X_{char}	char fraction in the pyrolysis products
57	ϕ_{bed}	bed porosity
58	ϕ_p	particle porosity
59	d_{cavity}	pore diameter
60	$D_{i,eff}$	effective diffusion coefficient of component (m^2/s)
61	ρ_m	mass concentration of component m (kg/m^3)
62	ρ	density of the fluid (kg/m^3)

M	molar mass kg/mol
ω_i	mass fraction of component i
$h_{i,eff}$	effective mass transfer coefficient
S_i	mass source (kg/m^3s)
x_k	molar fraction

1 Introduction

Anthropogenic climate change is forcing global society to increase the share of renewable sources in energy production. As a consequence, the combustion of lignocellulosic biomass for power generation as well as its conversion to biofuels has undergone a marked increase in recent years as it offers an attractive way to replace fossil fuels and to reduce net CO_2 emissions. However, the use of these bioresidues and their blends poses significant challenges due to variability in several critical factors including, composition, material density, devolatilization enthalpies and kinetics. Without special consideration in process design and operation, these inconsistencies may result in suboptimal conversion conditions for energy or fuel production. Furthermore, these variables can create disturbances to the plant operation resulting in economic losses, increased equipment wear and pollution. Thus, a large number of experimental studies on the thermal conversion of renewable fuels in a fixed-bed reactor, which allow replicating industrial conditions, have been reported in literature (Yang et al., 2007b).

Typically the experimental studies explore the effect of wood constituents on the pyrolysis mass loss dynamics and resultant products. For instance, Di Blasi et al. (2001) experimentally analyzed the weight loss dynamics of wood chips and determined that liquid and gaseous product yields were dependent on the content of holocellulose, while the char yield was specifically dependent on the lignin and extractives content. Burhenne et al. (2013) found that the increased lignin content of a biomass leads to slower decomposition rates, a higher devolatilization temperature and lower gas yield. Grønli (1996) also demonstrated that interparticular temperature gradients have a noticeable effect on the pyrolysis product yields. The results by Părpăriţă et al.

(2014) highlighted differences in the compositions of the bio-oils produced from different feedstocks: forestry biomass tends to produce more carboxylic acids, ketones and furans, but less phenolic compounds when compared to energy grass. The effect of heating rates has have also been examined and studies concerning pine (Williams and Besler, 1996) and pine bark (Şensöz, 2003) have shown that the effects of heating rates are less significant when compared to those of final temperature.

Although, experimental studies provide fundamental information on the pyrolysis of biomass, mathematical modeling allows an even deeper investigation of the underlying phenomena (Peters et al., 2003). However, only a limited number of studies on modeling of fixed bed pyrolysis have so far been reported. Cozzani et al. (1996) modeled the fixed-bed pyrolysis of milled refuse-derived fuel (RDF) with the aim of predicting product yields at different holding temperatures. Their results indicated that physical properties and variations in simulated wood composition had a more significant effect on the model predictions compared to other factors. In order to investigate thermal decomposition of beech wood, Peters et al. (2003) modeled packed bed pyrolysis of the material as an ensemble of separate particles, with each being described by a set of mass and energy conservation equations. The model was later extended by Mahmoudi et al. (2014) to also include effects of granular interactions and both these groups have demonstrated that this approach can adequately describe mass loss rate of a biomass sample. In contrast, Yang et al. (2007b) developed a fixed bed pyrolysis model for predicting product yields from devolatilization of wood, textile and cardboard residues, which assumed the competitive nature of gas, liquid and char formation processes. Results from the simulation indicated that the kinetic parameters determined for milled samples could not directly predict product yields in a packed bed and were optimized to fit experimental data. Anca-Couce et al. (2013) modelled fixed-bed pyrolysis of thick particles with a representative particle model (RPM) and their results suggested that particle diameter has a strong influence on the conversion time: doubling the diameter increases the time required for complete pyrolysis by 30 %. In the study by Lamarche et al. (2013), a pyrolysis model of a fixed bed reactor was employed in order to investigate the effect of fuel bed heat transfer resistance on the overall conversion process of the fuel. It was found that for the reactor configuration with a diameter of 10 cm used by researchers, high temperatures and long residence times were required in order to complete the devolatilization of the material.

113 However, thus far no attempt has been made to study the effect of physical factors like fuel bed density and
114 porosity on the pyrolysis yields at low heating rates in a fixed-bed reactor.

115 As a consequence, the aim of this study is to investigate the effect of fuel bed density and porosity as well as
116 various combinations of particle size and sweep gas flow on the pyrolysis product yields and their influence
117 on tar cracking. For these purposes, we develop a detailed dynamic model of fixed-bed pyrolysis which is
118 calibrated against the experimental data obtained in this study. The paper is structured as follows: Section 2
119 presents the material and the set-up for fixed-bed pyrolysis experiments. This is subsequently followed the
120 experimental results and analyzes (Section 3). In Section 4 the model and the determination of reaction rates
121 for primary and secondary reactions as well as reaction enthalpies and the validation of the model with the
122 determined reaction rates and enthalpies are all outlined. Section 5 presents the discussion and analysis before
123 finally, in Section 6, the results are summarized and the conclusions presented.

124 2 Materials and methods

125 2.1 Material

126 The material for the experiments was collected from the Metsä Wood Sawmill in Vilppula, Finland. The
127 debarking residue is composed of thin, irregularly shaped shavings of stem wood chips and spruce bark (3:7).
128 The particle size distribution of the material is presented in Table 1.

129 *Table 1 Particle size distribution of the debarking residue*

Size class, mm	Probability, %	Cumulative probability, %
0-3.15	20.1	20.1
3.15-8	22.6	42.7
8-16	26.4	69.1
16-45	29.9	99.1
45-63	0.9	100
63-100	0	100

100	0	100

130

131

2.2 Methods

2.2.1 Fixed-bed experiments

Prior to the fixed-bed experiments, the material was dried for two weeks at room temperature. In each experiment approximately 100 g of material was used and the sample was loaded into a sample basket which was then inserted into the reactor that comprised of a metal cylinder surrounded by a temperature controlled furnace. Temperature measurements were obtained from inside the fuel bed with three M-type thermocouples, at 11, 15 and 20 cm from the top of the reactor and data from these was logged every 4-5 seconds.

In the first two experiments, the samples were heated to a target temperature of 500 °C, in the third and fourth to 700 °C and in the final one 600 °C. All samples were heated at a pre-programmed wall heating rate of 6 °C/min and the material was held for one hour at the specified temperature with the exception of the first sample, which was held at the final temperature for three hours prior to switching off the furnace. In order to collect the condensable gases, the products from the pyrolysis reaction were directed into a water-cooled condenser with an exit that was connected to a glass flask immersed in icy water. This set-up allowed liquid phase samples to be collected into a glass bottle throughout the experiment. The hose from the bottle outlet was connected to a diverter T valve, and its two other outlets were connected to an extraction hood and to a gas collection bottle. The gas sample was collected only after the pyrolysing material reached the target temperature and nitrogen was used to purge the pyrolytic gas from the reactor at a rate of 2 l/min.

On completion of the experiment, the solid residue and the collected liquid samples were all weighed. The liquid product composition was analyzed with Perkin-Elmer GC-MS, 5% phenyl column (30 m x 0.25 mm x 0.25 um), where helium was the carrier gas (1 l/min). The oven temperature was programmed to rise from 60 to 260 °C at a rate of 10 K/min and then held at 260 °C for 10 min. The gaseous product composition was analyzed using a Varian CP 3800 gas chromatograph featuring a capillary column (CP sil 5, 5 um, 60 m x 0.32

mm) and helium carrier gas for hydrocarbon analysis. H_2, O_2, N_2, CO and CO_2 concentrations were quantified with a molecular sieve (packed bed columns, 1.5 m x 3.2 mm) and the carrier gas utilized was argon. The reactor set-up used in the experiments is presented in Fig. 1.

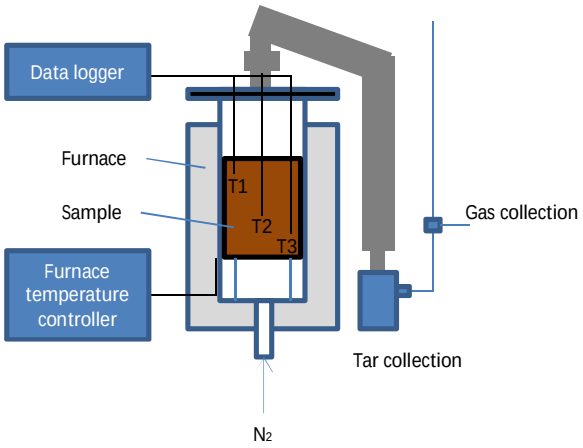

Fig. 1. Schematic of the small scale pyrolyser.

2.2.2 TGA experiments

The material used in the TG experiments was divided into two batches: one batch was air dried overnight at room temperature, whilst the second batch was dried in an oven at 90 °C for two weeks. Air-dried samples were cut into small pieces before the TGA tests, whereas the oven-dried batch was crushed in a Retsch PM100 ball mill and the subsequent powder obtained was sieved. The milled material was screened and separated into two batches, one with particles <500 µm (the largest share of which had a size less than 125 µm) and another with particles > 500 µm, which did not pass through the sieve due to their shape. The batch with particles > 500 µm consisted primarily of needle-shaped pure wood particles while, in contrast, the other batch contained both bark and wood powder. TGA was then performed on air-dried wood and bark samples, on both fractions of milled samples and on a mixture of the two milled fractions with a 2:5 ratio. In each experiment, the sample was heated to 900 °C at a heating rate of 80 K/min and the char yield was calculated as the ratio between the ash free sample weight at 900 °C and the ash free sample weight at 110 °C. Similarly, the moisture content was calculated as a ratio between the sample weight at 110 °C and the initial sample weight. The TG device used was a Perkin Elmer TGA 4000 and the experiments were performed under a nitrogen atmosphere (20 ml/min) with approximately 10 mg of the material used in each experiment.

3 Experimental results

Analysis of the results focused on determining the effect of final temperature on product yields, the composition of gaseous/liquid samples and the approximate composition of the solid residue. The analysis of the effect of the final temperature on pyrolysis product yields revealed a strong correlation: yields of solid and liquid products were inversely proportional to the temperature, as depicted in Fig. 2. The liquid phase yield showed a strong dependence on temperature while, in contrast, the solid phase yield had only a marginal dependence. The holding temperature not only affected the yield of liquid but also its composition - as outlined in Table 3. The most significant change in composition was observed during the transition from 600 to 700 °C that resulted in a higher phenolics concentration and increased the fraction of unknown compounds. Furthermore, the significantly lower content of anhydrosugars recorded at this temperature suggested that the conversion of cellulose derivatives was greater than at 500 or 600 °C. In addition, this observation suggests that in order for the anhydrosugars to undergo further conversion at 700 °C the residence time of these compounds has to be long enough. In addition to the decrease of anhydrosugars, the concentration of compound category M = 60 g/mol - the category which mainly comprised organic acids - also decreased. This observation was in marked contrast to the transition from 500 to 600 °C which influenced the concentrations of the liquid samples only slightly. The large difference in anhydrosugars content between 700 °C and 600 °C implies that the release of these components only occurs at rather elevated temperatures.

Table 2. Proximate analysis based on the TGA results

Sample	Volatile w% (d.a.f)	Char w% (d.a.f.)
Bark	72.95 %	27.05 %
Wood	82.06 %	17.94 %
Wood < 500 µm	78.13 %	21.87 %
Wood > 500 µm	81.70 %	18.30 %
Mixture	81.63 %	18.37 %

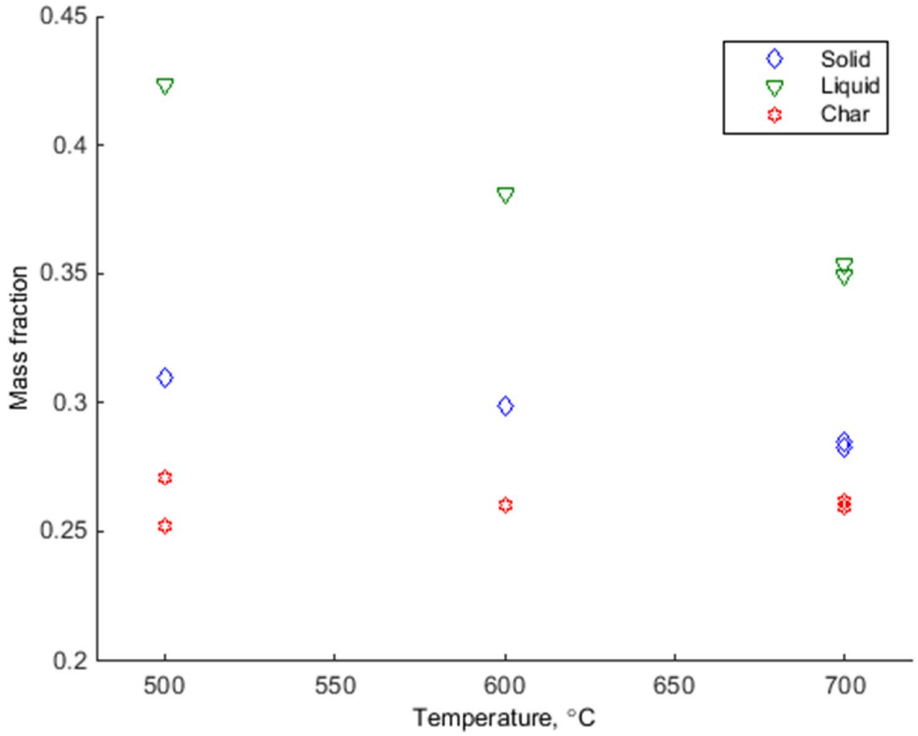

193

194 *Fig. 2. Liquid and solid product yields as a function of temperature*

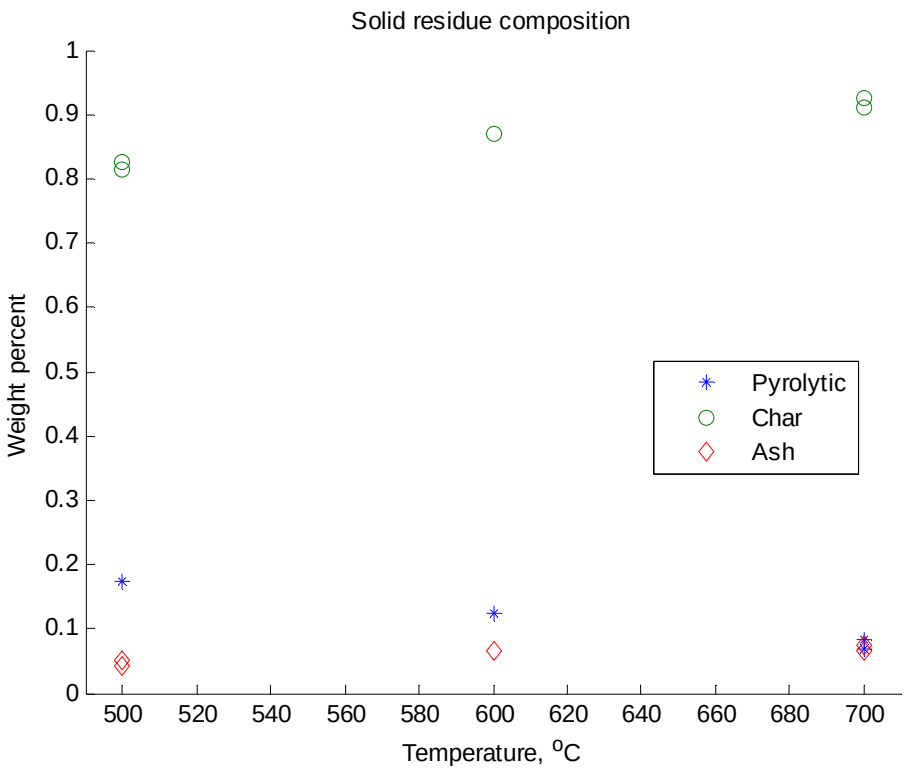

195

196 *Fig. 3. Volatile content of the pyrolyzed residue*

197

198

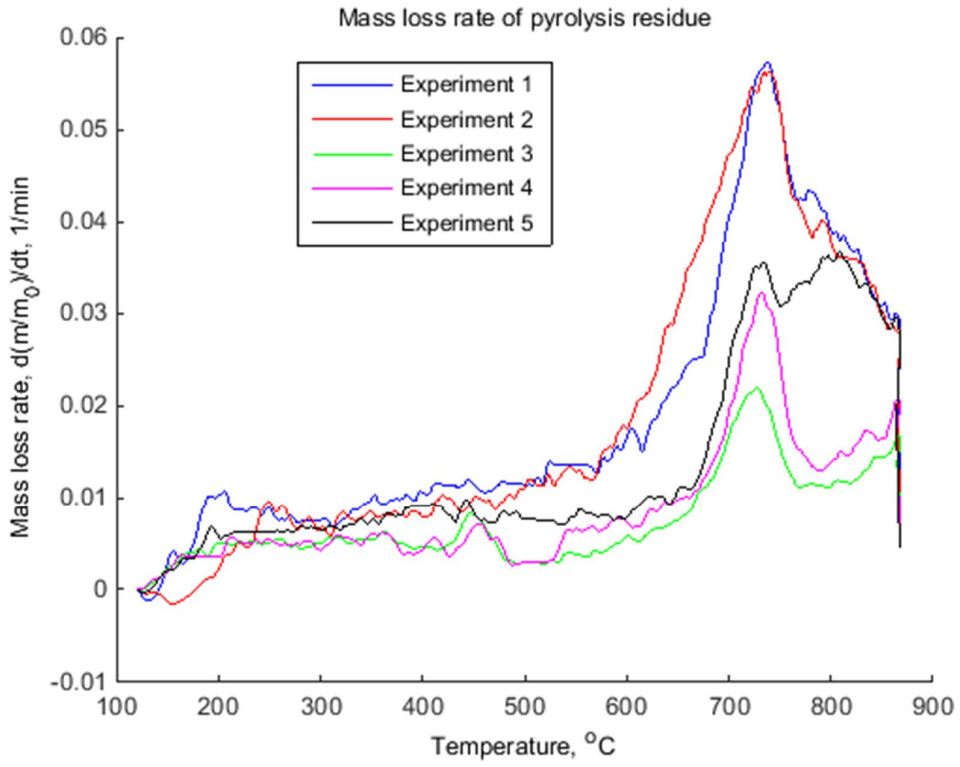

Fig. 4. Mass loss rate of the pyrolyzed material

Table 3. Composition of the liquids from the pyrolysis experiments

Category of compounds (w%)	500°C	500°C	600°C	700°C	700°C
Molecular weight M = 74	5.1	5.2	3.7	4.1	4.6
Molecular weight M = 60	29.1	28.7	32.7	10.6	11.1
Ketones	4.1	4.7	2.6	4.6	4.1
Substituted furans	9.1	10.3	10.1	11.8	12.3
Anhydrosugars	13.4	14.4	11.4	3.9	3.2
Phenolics	47.3	38.7	38.9	57.2	56.3
Unknown	2.3	2.6	2.1	10.4	9.8

The influence of the final pyrolysis temperature was also observed in the compositions of the gaseous product and the gaseous product compositions formed during the pyrolysis experiments are presented in Table 4. Analysis of gas indicated that temperatures of 500 and 600°C primarily promoted the formation of carbon dioxide and monoxide, whereas the transition to 700 °C caused a significant decrease in the production of CO_2, but had little effect on CO concentration. Moreover, the highest holding temperature yielded significantly

208 higher concentrations of hydrogen and methane, whilst also resulting in a marked decrease in C_3H_8
209 concentrations.

210 *Table 4 Gas composition from the pyrolysis experiments*

Temp	CO_2(%)	CO(%)	H_2 (%)	CH_4(%)	C_3H_8(%)
500	63.02	35.38	1.00	1.00	0.61
500	62.70	34.01	0.94	1.94	0.42
600	58.71	35.35	1.27	4.37	0.30
700	14.37	21.87	36.87	26.66	0.23
700	9.27	13.12	71.84	5.54	0.23

211

212 Solid residue collected from the experiments indicated that conversion of volatiles was not complete even at
213 700 °C. The residual pyrolytic content was found to be directly proportional to the final holding temperature,
214 as shown in Fig. 3. In addition, results from the thermogravimetric analysis of the solid residue (presented in
215 Fig. 4) indicated that each sample underwent further decomposition at temperatures higher than the holding
216 temperature.

217 **4** Mathematical model and the determination of reaction rates and
218 enthalpies

219 In order to properly take into account the decomposition of pyrolytic residue - illustrated in Fig. 4 - as well as
220 the heat of pyrolysis, the model was developed through calibration against the experimental data (Grieco and
221 Baldi, 2011;Park et al., 2010). Therefore, this section is divided into two parts: the first introduces the mass
222 and energy conservation equations, parameters and assumptions of the model; the other presents the
223 determination of the reaction rates and enthalpies with particular emphasis given to the decomposition of the
224 pyrolysis residue to tar and further tar cracking. Establishment of the reaction enthalpies for cellulose,
225 hemicellulose and lignin decomposition was also conducted in order to fit the measured temperature profiles.

4.1.1 Mathematical model

The fixed-bed pyrolysis model describes the mass loss rate of the fuel in a small-scale cylindrical pyrolysis reactor. In the model, the heat and mass transfer are governed by 2-D axisymmetric continuity equations while the overall pyrolysis reaction is divided into pseudo components that not only capture the pyrolysis kinetics of hemicellulose, cellulose and lignin but also the subsequent tar formation and cracking. The main equations of the model are presented in Table 6 and these include mass and energy conservation equations for the solid phase, described by Eqs. (1) and (2) and for the gas phase by Eqs. (14), and (21). In the gas phase, momentum conservation is considered by Eq. (13). The density of the gas phase only depends on temperature as shown by Eq. (19) whilst in contrast, the mass fractions of nitrogen and gaseous pyrolysis products are dependent on the rate of wood decomposition and tar cracking (Eq. (14)). The rate of tar cracking and mass transfer of tar between wood and gaseous phase is accounted for by Eq. (15).

Due to presence of thin particles and the low heating rate, the material can be approximated by a porous media assumption (Johansson et al., 2007) and thus internal temperature gradients are neglected. The overall heat conductivity of the bed is described by a correlation proposed by Yagi and Kunii (1957), which includes heat conduction between particles (Eq. (3)) , heat radiation between voids and particles (7) and void to void heat radiation (5). The heat conductivity of the solid phase (4) is assumed to comprise heat conduction – Eqs. (6) and (8) - and heat radiation, as outlined in Eqs. (9) and (11).

The tar formation and cracking kinetics determined by Rath and Staudinger (2001) were selected with the assumption that pyrolytic behavior of bark resembles that of spruce. A closer examination of the kinetics reported by Rath and Staudinger (2001) and mass loss kinetics by Garcia-Perez et al. (2007) revealed that the rate of formation for two of the tar categories observed (Rath and Staudinger, 2001) coincided with the decomposition rate of cellulose and hemicellulose, respectively. Thus, it was assumed that the decomposition kinetics of cellulose and hemicellulose can directly predict the formation of tar components *one* and *two*. Furthermore, since the formation of the third tar component occurred after the complete decomposition of cellulose and hemicellulose it was assumed that only lignin contributed to the formation of this component. Tar fractions were calculated from the values reported by Rath and Straudinger (2001) and were scaled by assuming the following debarking residue composition: cellulose 36 w%, hemicellulose 24 w% and lignin 40

253 w% (Garcìa-Pérez et al., 2007;Oasmaa et al., 2003). Based on the experimental results, it was presumed that
254 30 w% of the initial lignin content forms the intermediate solid. In total, the theoretical maximum liquid yield
255 in the model is 67 w% - an acceptable approximation as Oasmaa et al. (2010) have previously demonstrated
256 that fast-pyrolysis of forestry residues produces approximately 65 w% of liquid. In addition, it was assumed
257 that the mass transfer of tar from particle to the bulk fluid is controlled by pore diffusion (Eq. (22)). Chen et
258 al. (2013) have shown that this type of diffusion process is characterized by magnitudes in the region of 10^{-7},
259 therefore, based on this finding, the constriction factor of 0.01 and tortuosity coefficient of 15 were selected
260 as being appropriate for the model (Table 7). The gas composition from tar cracking, along with the cracking
261 kinetics, was selected from study by Rath and Straudinger (2001) who investigated tar formation and cracking.
262 Instead, the gas composition produced from cracking of tar formed in lignin pyrolysis was assumed to be
263 similar to gas released during Kraft pyrolysis measured by Ferdous et al. (2002).

264 The porosity was calculated to be 82 %. At the end of the experiments fuel bed height decreased to 30 – 40 %
265 of the initial while sample mass decreased to 29-33 % of the initial mass. This resulted in the porosity increase
266 of approximately 1-6 %. Therefore, the porosity was assumed constant, since, as demonstrated by Zou and Yu
267 (1996) and Porteiro and Patino (2010), bed porosity strongly depends on particle sphericity and only loosely
268 on particle size: for spheres of diameters below 20 mm the 40 % decrease in particle size results in
269 approximately 5 % porosity increase.

270 Results from the experiments suggested that the amount of forming char is independent of the final holding
271 temperature. The amount of char forming from each wood constituent was determined from the results by
272 Yang et al. (2007a), with the exception of cellulose for which the amount of char was assumed to be 15 w%
273 and Table 5 outlines the assumed product yields from each wood polymer. In addition, Table 9 presents the
274 kinetic parameters for the reactions considered by the model and Fig. 5 outlines the scheme devised for the
275 pyrolysis process.

276 The model based on the Finite Element Method was implemented in COMSOL 5.0 software package and the
277 time dependent kinetic and continuity equations were solved using the backward difference method (BDF).

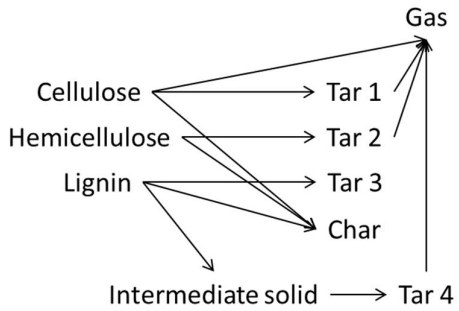

278

279 *Fig. 5. The proposed pyrolysis scheme for fixed-bed pyrolysis*

280 *Table 5. Weight fractions of the products released by wood constituents*

Precursor	Weight fraction			
	gas	tar	solid	Pyrolysis residue
CELL	0.15	0.7	0.15	0
HCELL	0	0.75	0.25	0
LIGNIN	0	0.3	0.40	0.3
Pyrolysis residue	0	1	0	0

281 *Table 6. Modeling equations of fixed bed pyrolysis*

Solid phase					
Mass continuity equation $\frac{\partial r_{m,i}}{\partial t} = -k_{m,i} r_{m,i}$				(1)	(Anon, 2014)
Energy continuity equation $(r C_p)\frac{\partial T_S}{\partial t} = \nabla \times (k_{bed} \nabla T_S) + Q$				(2)	(Anon, 2014)
Effective heat conductivity of the bed $\frac{k_{bed}}{k_g} = \frac{b(1-f_{bed})}{\left(\frac{k_g}{k_{s,eff}}\right) + \frac{1}{(1/j)+D_p k_{rs}/k_g}} + f_{bed} b \frac{D_p k_{rv}}{k_g}$	(3)	(Yagi and Kunii, 1957)	Effective heat conduction coefficient $k_{s.eff} = f_p k_{\max} + (1-f_p) k_{\min} + k_{s,rad}$	(4)	(Janssens and Douglas, 2004)
$k_{rv} = \frac{0.1952}{1+\frac{f_{bed}}{2(1-f_{bed})}} \frac{1-e}{e}\left(\frac{T}{100}\right)^3$	(5)	(Yagi and Kunii, 1957)	$k_{\min} = \frac{k_g k_{fiber}}{f_p k_{fiber} + (1-f_p) k_g}$	(6)	(Janssens and Douglas, 2004)
$k_{rs} = 0.1952\left(\frac{e}{1-e}\right)\left(\frac{T}{100}\right)^3$	(7)	(Yagi and Kunii, 1957)	$k_{\max} = f_p k_g + (1-f_p) k_{fiber}$	(8)	(Janssens and Douglas, 2004)
Radiative heat conductivity of wood particles $k_{s,rad} = \frac{4 f_p \sigma T_s^3 d_{cavity}}{1-f_p}$	(9)	(Janssens and Douglas, 2004)	Particle diameter $D_p = D_{p,0}(r_c + r_w)/r_{w,0}$	(10)	
Pore size $d_{cavity} = 3.5\times10^{-5}\sqrt{f_p}$	(11)	(Janssens and Douglas, 2004)	Particle porosity $f_p = 1-(r_w + r_c)/(1-f_{bed})/1500$	(12)	(Bryden and Hagge, 2003)
Gas phase					

Momentum conservation in the packed bed $\frac{\rho}{f_{bed}}\left(\frac{\partial \vec{u}}{\partial t}+(\vec{u}\cdot\nabla)\frac{\vec{u}}{f_{eb}}\right)=\nabla\cdot\left[-pI+\frac{\mu}{f_{bed}}\left(\nabla\vec{u}+(\nabla\vec{u})^{T}\right)-\frac{2\mu}{3f_{bed}}(\nabla\cdot\vec{u})I\right]-\left(\mu\kappa^{-1}+\beta_F\lvert\vec{u}\rvert+\frac{Q_{br}}{f_{bed}^{2}}\right)\vec{u}$				(13)	(Anon, 2014)
Gas phase mass continuity equation $f_{bed}\rho\frac{\partial w_i}{\partial t}-\nabla\cdot\left(\rho D_{i,eff}^{m}\nabla w_i+\rho w_i D_{i,eff}^{m}\frac{\nabla M_n}{M_n}+D_{i,eff}^{T}\frac{\nabla T}{T}\right)+\rho(\vec{u}\cdot\nabla)w_i=S_i$				(14)	(Anon, 2014)
Source term $S_i=-A_i\exp(-E_i/(RT))w_i\rho+h_{i,eff}S(\rho_{i,s}-w_i\rho)$	(15)	(Anon, 2014)	$D_{i,eff}=f_{bed}^{3/2}D_i$	(16)	(Anon, 2014)
Mass transfer coefficient $h_{eff,i}=(2+0.6\times(\mu/D_e)^{1/3}\mathrm{Re}^{0.5})/D_p\times D_e$	(17)	(Wakao et al., 1979)	Average molar mass of the fluid $M_n=\left(\sum_i\frac{w_i}{M_i}\right)$	(18)	(Anon, 2014)
Mass conservation of the fluid $\frac{\partial\rho}{\partial t}+\nabla\cdot(\rho\vec{u})=0$	(19)	(Anon, 2014)	Diffusion coefficient $D_i=\frac{1-w_i}{\sum_{k\neq i}\frac{x_k}{D_{ik}}}$	(20)	(Anon, 2014)
Energy continuity equation $\rho C_p\frac{\partial T_g}{\partial t}+\rho C_p\vec{u}\cdot\nabla T_g=\nabla\cdot(k\nabla T_g)+Q$	(21)	(Anon, 2014)	Effective diffusion coefficient $D_e=\frac{D_i f_p \sigma_c}{\tau}$	(22)	(Fogler, 2006)

Table 7. Parameters used in the model

Wood heat capacity	2400 kJ/kg/K	(Shin and Choi, 2000)
Char heat capacity	$-0.0038T^2 + 5.98T - 795.28$	(Gupta et al., 2003)
Wood heat conductivity	0.35 W/m/K	(Grønli and Melaaen, 2000)
Char heat conductivity	0.1 W/m/K	(Grønli and Melaaen, 2000)
Bed porosity	0.82	
Wood emissivity	0.7	(Corbetta et al., 2014)
Char emissivity	0.92	(Corbetta et al., 2014)
σ_c	0.01	
τ	15	

4.1.2 Determination of reaction rates and reaction enthalpies for the model

Reaction rates for the decomposition of pyrolytic residue and tar cracking

A sensitivity analysis was performed in order to determine the decomposition of the intermediate solid to tar and tar cracking. Based on the results from the TGA experiments conducted on the pyrolyzed residue, three alternative reaction rates were selected with maximum decomposition rates in the vicinity of 550, 650 and 750 °C. For the tar cracking reaction, rate equations with activation energies of 160, 200 and 240 kJ/mol

respectively, were chosen and the combinations of the considered kinetic parameters for the rate equations of solid and tar decomposition are outlined in Table 8. The results from the sensitivity analysis (Fig. 6) were then compared with tar and solid yields resulting from the experiments conducted at 873 and 973 K while the data from the experiment at 773 K was used for validation purposes. The results from the analysis suggested that combination number 5 in Table 8 provided the best fit for both liquid and solid product yields.

Table 8. Combinations of the kinetic parameters for the mass loss rates of solid and tar

		Residue decomposition		
		8.7 s^{-1}, 60 kJ/mol	40 s^{-1}, 80 kJ/mol	150 s^{-1}, 100 kJ/mol
Tar decomposition	2´ 10^9 s^{-1}, 160 kJ/mol	1	4	7
	5´ 10^{10} s^{-1}, 200 kJ/mol	2	5	8
	1´ 10^{12} s^{-1}, 240 kJ/mol	3	6	9

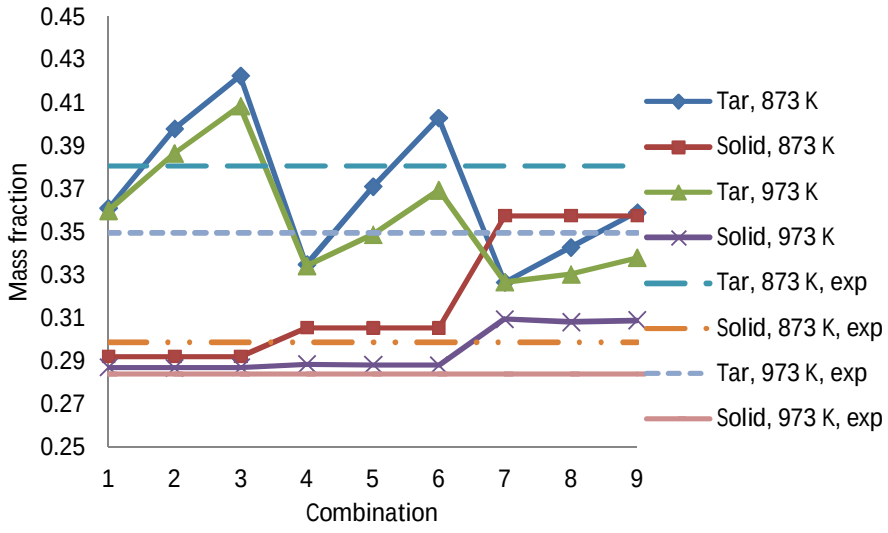

Fig. 6. Product yields for each combination of the kinetic parameters

Table 9 Summary of the kinetic parameters used in the model

	A	E (kJ/kg)	n

Cellulose pyrolysis	k_{cell}	$8.75x10^{18}$ (min^{-1})	233	1	(Garcìa-Pérez et al., 2007)
Hemicellulose pyrolysis	k_{hcell}	$5x10^{8}$ (min^{-1})	105	1	(Garcìa-Pérez et al., 2007)
Lignin pyrolysis	k_{lignin}	25 (min^{-1})	30	1.12	(Garcìa-Pérez et al., 2007)
Tar 3 formation from lignin	k_{T3}	$3.02x10^{21}$ (g/mg/s)	320.2	2	(Rath and Staudinger, 2001)
Tar 1 cracking	k_{T1g}	$3.076x10^{3}$ (s^{-1})	66.3	1	(Rath and Staudinger, 2001)
Tar 2 cracking	k_{T2g}	$1.130x10^{6}$ (s^{-1})	109	1	(Rath and Staudinger, 2001)
Tar 4 formation from intermediate solid	$k_{ss\text{-}liqss}$	40 (s^{-1})	80	1	this study
Cracking of Tar 4	$k_{liqss\text{-}g}$	$5x10^{10}$ (s^{-1})	200	1	this study

Reaction enthalpies for primary pyrolysis reactions

The reaction enthalpies were determined by simulating the combinations of the following reaction heats: lignin -400, -600, -1000 kJ/kg, cellulose: 0, -100 kJ/kg, hemicellulose: 0, -100, -200 kJ/kg. Additionally, it was also assumed that the conversion of pyrolysis residue to tar and further tar cracking have neutral pyrolysis heat. A simulated temperature profile at the location of TC2 was then compared with the measurement by calculating the residual sum of squares (RSS) index and it found that the estimated reaction heats of -100 kJ/kg for cellulose, -200 kJ/kg for hemicellulose and -600 kJ/kg for lignin, in total yielding -304 kJ/kg for the fuel, provided a good fit between the predicted experimental profile with the measured one. The RSS index for each combination is reported in Fig. 7, which also presents the comparison of the combination with the smallest RSS and the measured temperature of the second thermocouple. The obtained value is in line with the reaction heats previously reported in the literature for exothermic heats of wood pyrolysis: 245 and 418 kJ/kg (Koufopanos et al., 1991), (Bilbao et al., 1993), (Roberts, 1971). Although the exothermic value for cellulose decomposition is subject to some debate in the literature, work by Arseneau (1971) has shown that for mass-transfer-limited conditions, the primary decomposition reaction of cellulose overlaps with levoglucosan decomposition (one of the cellulose pyrolysis products) which results in an exothermic cellulose pyrolysis reaction.

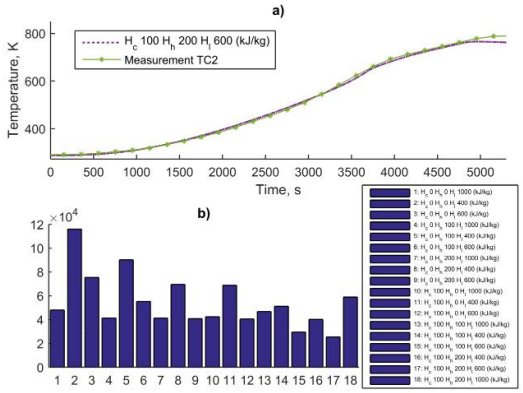

Fig. 7. a) Comparison of the measured and simulated temperature profile; b) RSE indexes for the combinations of reaction heats for primary pyrolysis

Validation of the model with the determined reaction rates and enthalpies

The value obtained for pyrolysis enthalpy was incorporated into the model and the subsequent prediction was validated against the measurements of all three thermocouples in experiments at three temperatures. Overall, the model demonstrated a satisfactory accuracy, however, some discrepancies were observed for the TC3 measurement that was located closer to the center of the bed and was thus affected by the gas flow more significantly than the other two thermocouples. The simulated gas profile suggested that the variations observed in TC3 between different experiments were caused by a channeling effect within the fuel bed. Such a channeling effect probably resulted from the particle orientation within the bed, since at locations close to the bottom of the sample basket even a single particle can cause a large variation in the temperature profile. This observation is supported by the fact that the simulated temperature of the gas flow at distances within one particle diameter from the TC3 coincided with the measured temperatures as presented in Fig. 8. The rapid change in the heating rate of the experiment conducted at 500 °C was presumed to result from particle

reorientation due to particle diameter decreases that occurred during the conversion process.

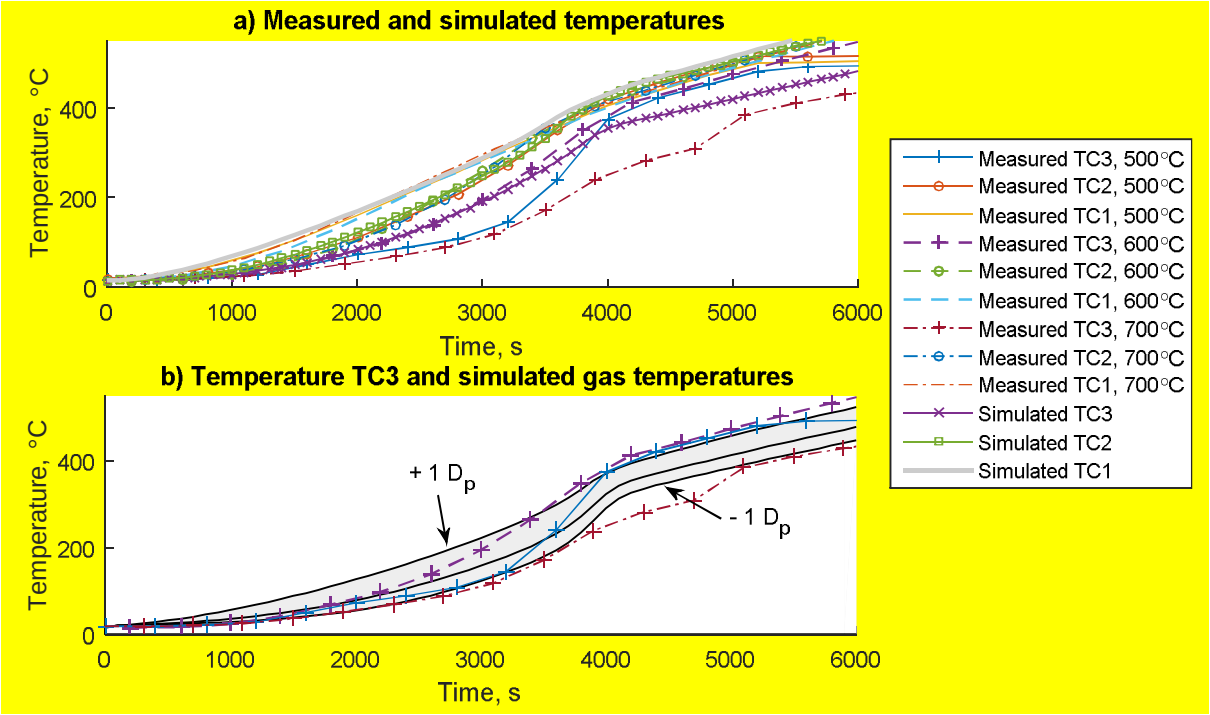

Fig. 8. a) Measured and predicted temperature profiles of the fixed bed experiments, experiment at 500 ℃ (solid), 600 ℃ (dash-dot) and 700 ℃ (dashed line), measurements TC3 (+), TC2 (o) and TC1 no marker. Simulated TC3 (x), TC2 (□) and TC1 solid thick line. b) The comparison of measured temperatures TC3, (500, 600 and 700 ℃) and simulated gas temperatures at coordinates of TC3 ± 1D_p (one particle diameter from)

The product yields predicted by the model were also validated against the measured ones and the predicted product yields showed a good correlation with the measured values, including those at 773 K which were not used for determination of reaction rates. Although no measured values were available for 673 K, the predicted trend for the liquid yield resembles those previously reported for spruce wood: tar yield increases until 500 °C where it reaches maximum and starts slowly decreasing as temperature increases further (Demirbas, 2010). Furthermore, for spruce bark pyrolysis, Demirbas (2010) has reported average values of 36.3 w% and 35.2 w% for bio-oil and char yields respectively, in the temperature range from 350 to 600 °C (no temperature specific values were provided). When the same temperature range was utilized as a basis for the model outlined here, it predicted average bio-oil and solid yields of 34.9 w% and 36 w%, respectively. This comparison against both the experimental results and the values provided in the literature clearly demonstrates that the model has satisfactory levels of accuracy. In addition, the calculated Biot number suggests the adequacy of the thermally

thin particle assumption. The Biot number, presented in Fig. 10, remains below the stringent limit of 0.2 (Piskorz et al., 2000) most of the time and always << 1 (Di Blasi, 1996).

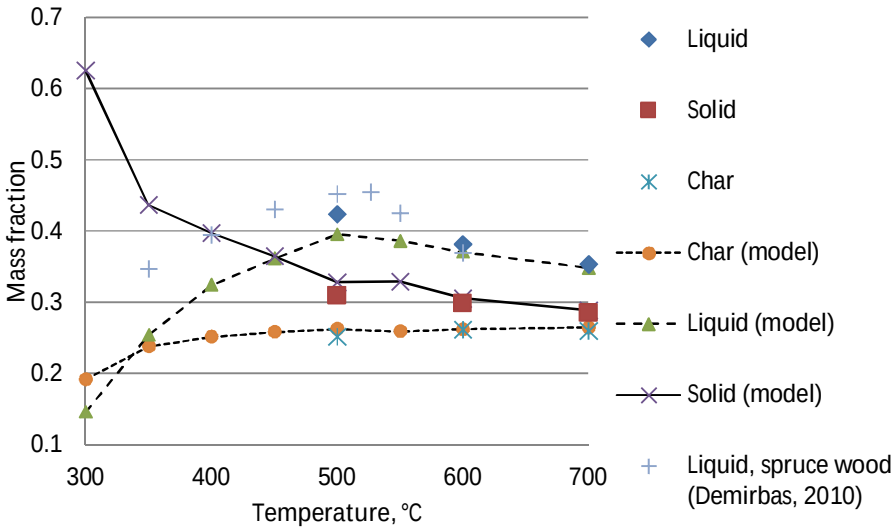

Fig. 9. Liquid, solid and char yields predicted by the model

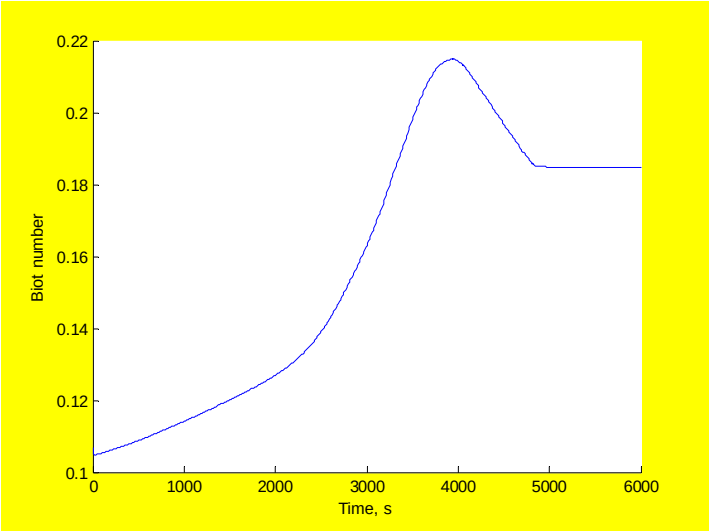

Fig. 10 Biot number evolution during the simulation

5 Analysis and discussion

Analysis of the factors influencing the product yields investigated the effect of particle diameter, nitrogen flow, bed density and porosity on product yields. The results from the analyses - which were all simulated up to

360 10000 seconds - are presented in Fig. 11, Fig. 12 and Fig. 13. One of the most important variables in the
361 thermal conversion of biomass is the particle diameter as it controls heat and mass transfer inside the bed.
362 Decreasing particle size improves mass transfer, but subjects the fuel to an increasing cooling effect from gas
363 flow. Tar yields demonstrated this dependence and increased as particle size decreased, nevertheless at the
364 highest flow rate tar yield, differences were found to be minimal between the two smallest particle sizes
365 investigated. A comparison between the gas phase and intraparticle tar cracking, presented in Fig. 12, indicated
366 that gas flow affects tar decomposition in both phases. Higher gas flow rates improve the tar flow out of the
367 particles by decreasing the tar concentration in the gas surrounding the material and thus diminishes the amount
368 of tar cracking inside the particles. In contrast, the amount of tar cracking in the gas phase is almost independent
369 of sweeping gas flow but it is, to a large degree, dependent on the particle size. Thus, the increased tar
370 concentration in the gas phase for higher flows and subsequently larger magnitudes of cracking reactions
371 compensate the effect of increased gas velocity. However, despite the beneficial impact of high gas flows on
372 the tar content, these cool the fuel bed and prevent the material at the bottom of the bed from reacting, an effect
373 that is clearly demonstrated by the increased solid yield for higher flow rates. As a result smaller particle
374 diameters require longer holding times and temperatures in order to achieve the complete conversion,
375 especially, in the center of the fuel bed as was observed by Lamarche et al. (2013). Consequently, preheating
376 of the sweeping gas can offer an effective way to increase tar yields for smaller particle sizes by countering
377 the cooling effect. Nevertheless, gas preheating along with the energy required for particle size reduction may
378 decrease the overall efficiency of the pyrolysis process and as a result the use of large particle sizes may prove
379 more beneficial when compared to smaller particles, for example, the largest particle size (15 mm)
380 demonstrated only an insignificant dependence of solid yield on gas flow.

381 Bed density and porosity also demonstrated a strong influence on product yields (Fig. 13) due to their effect
382 on heat transfer. This is shown in Fig. 14, which compares the effective heat conduction coefficients of the
383 bed and wood of the fuel bed for the highest and lowest porosities. The average heat conduction coefficients
384 were calculated by averaging the coefficients given by Eqs. (3) and (4) over the computational domain. The
385 results revealed that the lowest porosity produced significantly more liquid (42 w%) when compared to the
386 case with the highest porosity (35 w%). These differences in the liquid yields originated from the tar cracking

inside the particles that for the lowest bed porosity was approximately 26 % lower than for the highest porosity even though the fraction of tar cracking in the gas phase was equal for flows of 1 and 3 l/min. In addition, the material with the highest porosity reached the maximum tar yield at 773 K, while lower porosities tended to increase liquid yields with temperature. Furthermore, as porosity increased, a larger increase in the liquid yield was achieved with the increase in holding temperature.

In contrast to the liquid yield, the solid as well as the char yield were unaffected by both the porosity and bed density, since yields of these products were mainly dependent on the holding temperature and time. The results show that high bed porosities result in lower heat conductivity at temperatures where the heat radiation is insignificant as under these conditions, the heat transfer occurs to a large extent through the contact surface between particles and the gas populating the void spaces of the bed. Moreover, due to lower density, the heat conductivity of the fuel bed with higher porosity initially tends to increase slightly more rapidly than with the lowest one. In contrast, in denser fuels the effect of pyrolysis heat becomes more noticeable as the mass concentration of wood increases, the exothermic effect is shown in Fig. 14 as an overshoot in the heat transfer coefficient occurring after 5000 seconds. However, during the active pyrolysis phase - which occurs in the range between 3000 and 4000 seconds - the less dense fuel bed underwent a larger decrease in thermal conductivity as intraparticle porosity increased. Horttanainen et al. (2002) observed a similar effect: lower fuel bed porosities improved heat transfer inside the bed and increased the velocity of reaction front propagation. Thus, the results indicate that low bed porosities are desirable in order to maximize the yield of liquid products.

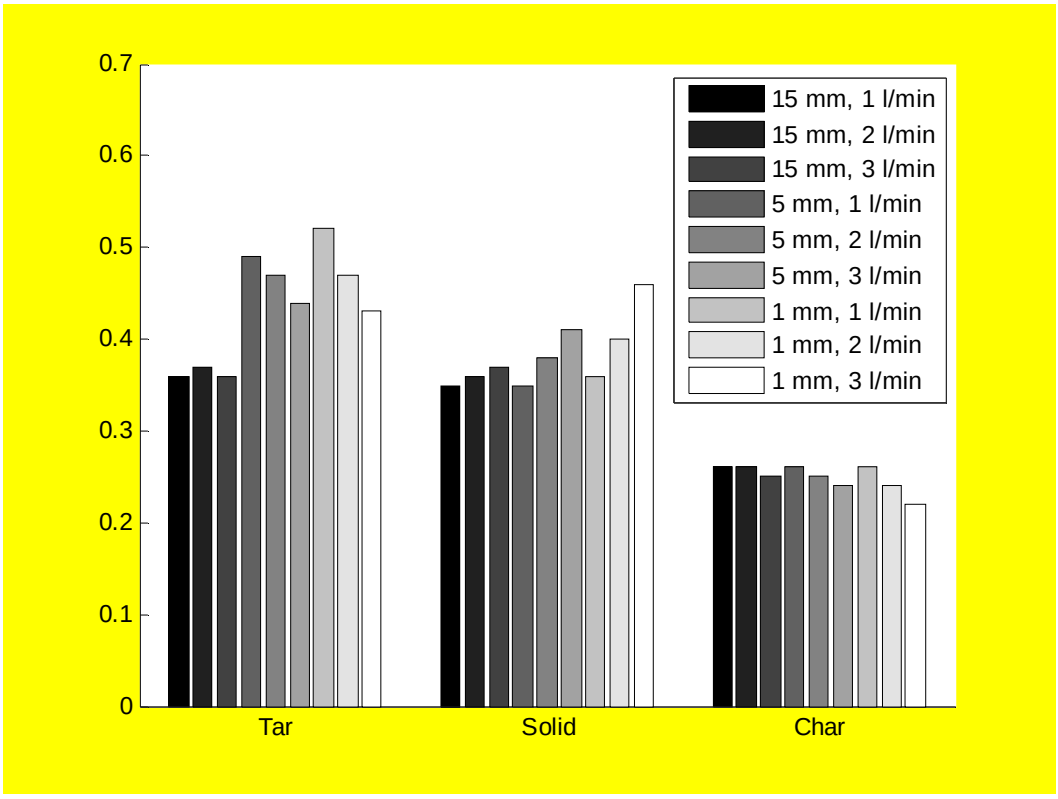

405

406 *Fig. 11 Product yields for different combinations of particle diameters and gas flow*

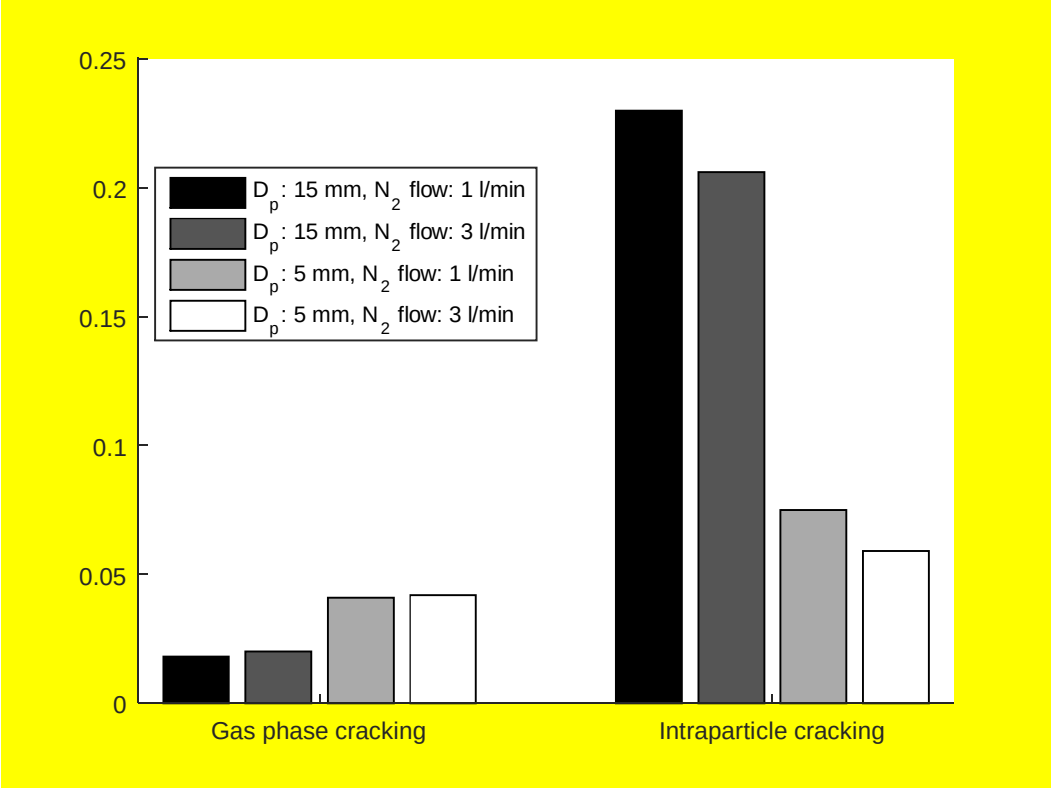

407

408 *Fig. 12 Effect of particle size and nitrogen flow on tar cracking*

409

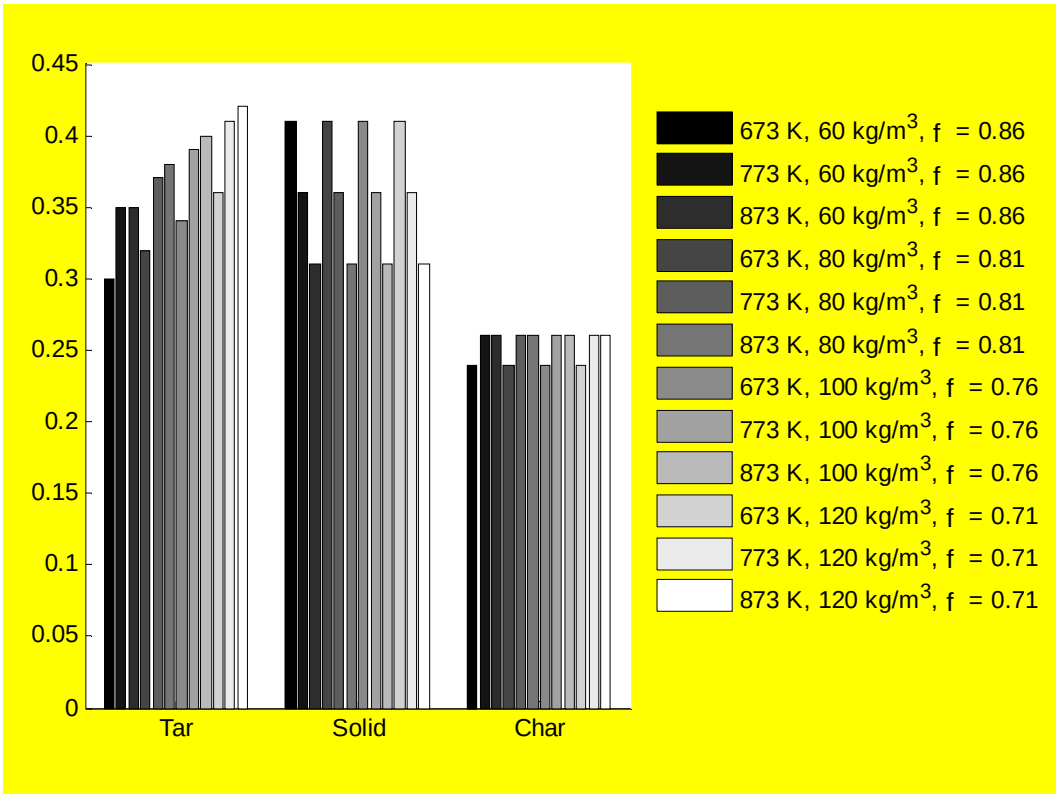

410

411 *Fig. 13 Effect of bed density and porosity on the product yields*

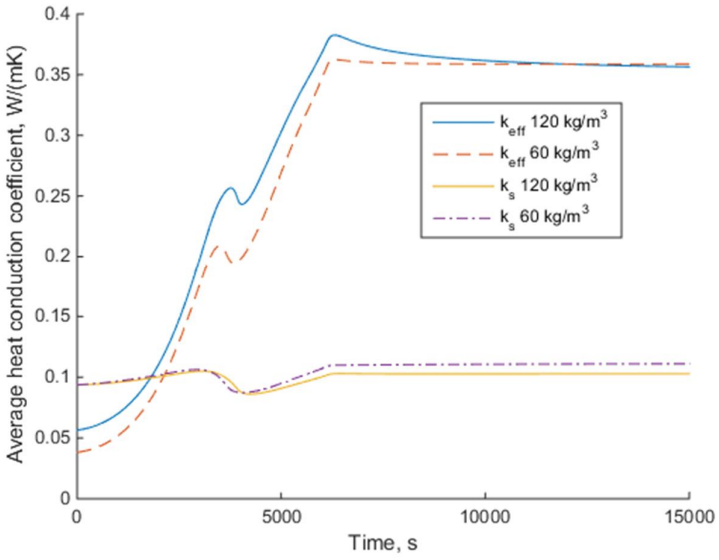

412

413 *Fig. 14. Effect of bed porosity on the heat conductivity of the fuel bed*

6 Conclusions

The aim of this study was to investigate the effect of the physical parameters of fuel on pyrolysis product yields and tar cracking. Experimental results obtained in the study showed that liquid and solid yields decreased as the temperature was increased. Although the increase in the holding temperature produced a lower amount of solid residue, the amount of char within the residue remained constant despite different holding temperatures. The simulation results indicated that decreasing particle diameter and increasing gas flow rate results in larger mass fractions of liquid, however, these parameters also increased the fraction of the unreacted solid due to the increased cooling effect from the sweeping nitrogen. Therefore, close attention needs to be paid when selecting the appropriate combination of particle size and sweep gas flow as a small particle size combined with high flow rates increases the liquid yield but results in a larger quantity of the unreacted material. Furthermore, decreasing bed porosity resulted in higher liquid yields, but did not affect the solid and char yield, thus it can be concluded that higher bed densities (lower bed porosities) favor liquid production.

Overall, the results presented in this paper provide valuable information on the fixed-bed pyrolysis of the spruce debarking residue (*Picea abies*) which is the fuel widely utilized for power production in Finland and Scandinavia. This knowledge can be utilized for the optimization of combustion and pyrolysis processes, for example, BioGrate boilers that operate under co-current combustion conditions resulting in fuel pyrolysis under oxygen-free conditions (Boriouchkine et al., 2012).

ACKNOWLEDGEMENTS

This work was partially supported by the ICBCOM consortium project of the Finnish Funding Agency for Technology and Innovation (TEKES). The first author would like to thank Graduate School in Chemical Engineering in Finland, and Walter Ahlström foundation for the financial support.

REFERENCES

Anca-Couce, A., Zobel, N., Jakobsen, H. A., 2013. Multi-scale modeling of fixed-bed thermo-chemical processes of biomass with the representative particle model: Application to pyrolysis, Fuel 103(0), 773-782.

439 Anon, 2014. Manual, Version 5.0. Burlington, USA: Comsol Multiphysics.

440 Arseneau, D. F., 1971. Competitive Reactions in the Thermal Decomposition of Cellulose, Canadian Journal
441 of Chemistry 49(4), 632-638.

442 Bilbao, R., Millera, A., Murillo, M. B., 1993. Temperature profiles and weight loss in the thermal
443 decomposition of large spherical wood particles, Industrial & Engineering Chemistry Research 32(9), 1811-
444 1817.

445 Boriouchkine, A., Zakharov, A., Jämsä-Jounela, S., 2012. Dynamic modeling of combustion in a BioGrate
446 furnace: The effect of operation parameters on biomass firing, Chemical Engineering Science 69(1), 669-
447 678.

448 Bryden, K. M., Hagge, M. J., 2003. Modeling the combined impact of moisture and char shrinkage on the
449 pyrolysis of a biomass particle☆, Fuel 82(13), 1633-1644.

450 Burhenne, L., Messmer, J., Aicher, T., Laborie, M., 2013. The effect of the biomass components lignin,
451 cellulose and hemicellulose on TGA and fixed bed pyrolysis, Journal of Analytical and Applied Pyrolysis
452 101(0), 177-184.

453 Chen, Y., Wang, X., Cao, L., He, R., 2013. Effects of Fractal Pore on Coal Devolatilization, in: Qi, H., Zhao,
454 B. (Eds), , Springer Berlin Heidelberg, pp. 175-180.

455 Corbetta, M., Frassoldati, A., Bennadji, H., Smith, K., Serapiglia, M. J., Gauthier, G., Melkior, T., Ranzi, E.,
456 Fisher, E. M., 2014. Pyrolysis of Centimeter-Scale Woody Biomass Particles: Kinetic Modeling and
457 Experimental Validation, Energy Fuels 28(6), 3884-3898.

458 Cozzani, V., Nicolella, C., Rovatti, M., Tognotti, L., 1996. Modeling and Experimental Verification of Physical
459 and Chemical Processes during Pyrolysis of a Refuse-Derived Fuel, Industrial & Engineering Chemistry
460 Research 35(1), 90-98.

461 Demirbas, M. F., 2010. Characterization of Bio-oils from Spruce Wood (Picea orientalis L.) via Pyrolysis,
462 Energy Sources, Part A: Recovery, Utilization, and Environmental Effects 32(10), 909-916.

463 Di Blasi, C., 1996. Kinetic and heat transfer control in the slow and flash pyrolysis of solids, Industrial &
464 Engineering Chemistry Research 35(1), 37-46.

465 Di Blasi, C., Branca, C., Santoro, A., Perez Bermudez, R. A., 2001. Weight loss dynamics of wood chips
466 under fast radiative heating, Journal of Analytical and Applied Pyrolysis 57(1), 77-90.

467 Ferdous, D., Dalai, A. K., Bej, S. K., Thring, R. W., 2002. Pyrolysis of Lignins: Experimental and Kinetics
468 Studies, Energy Fuels 16(6), 1405-1412.

469 Fogler, S., 2006. Elements of Chemical Reaction Engineering, 4. Ed. Upper Saddle River, USA: Pearson
470 Educations.

471 Garcìa-Pérez, M., Chaala, A., Pakdel, H., Kretschmer, D., Roy, C., 2007. Vacuum pyrolysis of softwood and
472 hardwood biomass: Comparison between product yields and bio-oil properties, Journal of Analytical and
473 Applied Pyrolysis 78(1), 104-116.

474 Grieco, E., Baldi, G., 2011. Analysis and modelling of wood pyrolysis, Chemical Engineering Science 66(4),
475 650-660.

476 Grønli, M. G., Melaaen, M. C., 2000. Mathematical Model for Wood PyrolysisComparison of Experimental
477 Measurements with Model Predictions, Energy Fuels 14(4), 791-800.

478 Grønli, M. G., 1996. A theoretical and experimental study of the thermal degradation of biomass,.

479 Gupta, M., Yang, J., Roy, C., 2003. Specific heat and thermal conductivity of softwood bark and softwood
480 char particles☆, Fuel 82(8), 919-927.

481 Horttanainen, M., Saastamoinen, J., Sarkomaa, P., 2002. Operational Limits of Ignition Front Propagation
482 against Airflow in Packed Beds of Different Wood Fuels, Energy Fuels 16(3), 676-686.

483 Janssens, M., Douglas, B., 2004. Wood and wood products, in: Harper, C. (Ed), Handbook of Building
484 Materials for Fire Protection. New-York, McGraw-Hill, pp. 1-58.

485 Johansson, R., Thunman, H., Leckner, B., 2007. Influence of intraparticle gradients in modeling of fixed
486 bed combustion, Combustion and Flame 149(1–2), 49-62.

487 Koufopanos, C. A., Papayannakos, N., Maschio, G., Lucchesi, A., 1991. Modelling of the pyrolysis of biomass
488 particles. Studies on kinetics, thermal and heat transfer effects, The Canadian Journal of Chemical
489 Engineering 69(4), 907-915.

490 Lamarche, P., Tazerout, M., Gelix, F., Köhler, S., Mati, K., Paviet, F., 2013. Modelling of an indirectly heated
491 fixed bed pyrolysis reactor of wood: Transition from batch to continuous staged gasification, Fuel 106(0),
492 118-128.

493 Mahmoudi, A. H., Hoffmann, F., Peters, B., 2014. Detailed numerical modeling of pyrolysis in a
494 heterogeneous packed bed using XDEM, Journal of Analytical and Applied Pyrolysis 106(0), 9-20.

495 Oasmaa, A., Kuoppala, E., Gust, S., Solantausta, Y., 2003. Fast Pyrolysis of Forestry Residue. 1. Effect of
496 Extractives on Phase Separation of Pyrolysis Liquids, Energy Fuels 17(1), 1-12.

497 Oasmaa, A., Solantausta, Y., Arpiainen, V., Kuoppala, E., Sipilä, K., 2010. Fast Pyrolysis Bio-Oils from
498 Wood and Agricultural Residues, Energy Fuels 24(2), 1380-1388.

499 Park, W. C., Atreya, A., Baum, H. R., 2010. Experimental and theoretical investigation of heat and mass
500 transfer processes during wood pyrolysis, Combustion and Flame 157(3), 481-494.

501 Părpăriţă, E., Brebu, M., Azhar Uddin, M., Yanik, J., Vasile, C., 2014. Pyrolysis behaviors of various
502 biomasses, Polymer Degradation and Stability 100(0), 1-9.

503 Peters, B., Schröder, E., Bruch, C., 2003. Measurements and particle resolved modelling of the thermo-
504 and fluid dynamics of a packed bed, Journal of Analytical and Applied Pyrolysis 70(2), 211-231.

505 Piskorz, J., Majerski, P., Radlein, D., Vladars-Usas, A., Scott, D. S., 2000. Flash pyrolysis of cellulose for
506 production of anhydro-oligomers, Journal of Analytical and Applied Pyrolysis 56(2), 145-166.

507 Porteiro, J., Patiño, D., Collazo, J., Granada, E., Moran, J., Miguez, J. L., 2010. Experimental analysis of
508 the ignition front propagation of several biomass fuels in a fixed-bed combustor, Fuel 89(1), 26-35.

509 Rath, J., Staudinger, G., 2001. Cracking reactions of tar from pyrolysis of spruce wood, Fuel 80(10), 1379-
510 1389.

511 Roberts, A. F., 1971. The heat of reaction during the pyrolysis of wood, Combustion and Flame 17(1), 79-
512 86.

513 Şensöz, S., 2003. Slow pyrolysis of wood barks from Pinus brutia Ten. and product compositions,
514 Bioresource technology 89(3), 307-311.

515 Shin, D., Choi, S., 2000. The combustion of simulated waste particles in a fixed bed, Combustion and Flame
516 121(1–2), 167-180.

517 Wakao, N., Kaguei, S., Funazkri, T., 1979. Effect of fluid dispersion coefficients on particle-to-fluid heat
518 transfer coefficients in packed beds: Correlation of nusselt numbers, Chemical Engineering Science 34(3),
519 325-336.

520 Williams, P. T., Besler, S., 1996. The influence of temperature and heating rate on the slow pyrolysis of
521 biomass, Renewable Energy 7(3), 233-250.

522 Yagi, S., Kunii, D., 1957. Studies on effective thermal conductivities in packed beds, AIChE Journal 3(3),
523 373-381.

524 Yang, H., Yan, R., Chen, H., Lee, D. H., Zheng, C., 2007a. Characteristics of hemicellulose, cellulose and
525 lignin pyrolysis, Fuel 86(12–13), 1781-1788.

526 Yang, Y. B., Phan, A. N., Ryu, C., Sharifi, V., Swithenbank, J., 2007b. Mathematical modelling of slow
527 pyrolysis of segregated solid wastes in a packed-bed pyrolyser, Fuel 86(1–2), 169-180.

528 Zou, R. P., Yu, A. B., 1996. Evaluation of the packing characteristics of mono-sized non-spherical particles,
529 Powder Technology 88(1), 71-79.

530